Heritage Science

RESEARCH

Open Access

Desalination of *Hamipterus tianshanensis* fossil by electrokinetic method: evaluation for treatment of clay-rich sandstone

Ying Li[1,2,3], Yimin Yang[2,3], Xiaolin Wang[3,4*] and Wugan Luo[2,3*]

Abstract

The fossils of *Hamipterus tianshanensis* (Wang et al. in Curr Biol 24:1323–1330, 2014) and their eggs have important scientific significance because they can provide unique information about the reproduction, development, and evolution of pterosaurs. The fossils and the rock surrounding them have, however, been weathered, which including powdering and flaking, since they were relocated from Xinjiang to Beijing. The high content of soluble salts is a significant factor in fossil deterioration because the dissolution–recrystallization process can generate tremendous pressure and lead to decreased mechanical strength. This study evaluated the electrokinetic desalination performance for the fossils, and two types of poultices employed including paper pulp from Bioline® and CKS121 (cellulose: kaolin: sand = 1:2:1, w/w). Mercury intrusion porosimetry (MIP), scanning electron microscopy (SEM), ion chromatography (IC), and other methods were applied to evaluate the desalination effect. The surface salt content reduction by applied direct current (DC) was about 70%, and the inner salt content reduction was about 80%. The experimental results suggest that the electrokinetic method is a promising way to desalinate fossils. Nonetheless, cracks appeared in the surrounding rock crack after electrokinetic desalination, which can be explained by the montmorillonite swelling-induced stresses. Pre-consolidation, especially for electro-chemical method may solve the cracking problem for the clay-rich sandstone desalination.

Keywords Salt weathering, Desalination, Electrochemistry, Fossil matrix, Poultice, Pore size distribution

Introduction

Fossils are nonrenewable natural heritages and provide clues about changes in the world's species. By studying fossils, scientists can learn more about the earth's past, which may lead to better predictions for future development. The Turpan-Hami Basin, Xinjiang, China, is unique among sites with numerous fossils. This site preserves many bones, eggs, and even embryos of pterosaur in three dimensions (3D). However, three-dimensional pterosaurs are rarer compared to two-dimensional or flattened ones. After years of investigation and research, these fossils have been reported as a population of a new sexually dimorphic pterosaur species (*Hamipterus tianshanensis*) [1]. The discovery of *H. tianshanensis* is of great value to paleontologists, as the findings shed new light on the reproductive

*Correspondence:
Xiaolin Wang
wangxiaolin@ivpp.ac.cn
Wugan Luo
xiahua@ucas.edu.cn
[1] Institute of Archaeology, Chinese Academy of Social Science, Beijing 100101, China
[2] Department of Archaeology and Anthropology, University of Chinese Academy of Sciences, Beijing 100049, China
[3] Key Laboratory of Vertebrate Evolution and Human Origins of Chinese Academy of Sciences, Institute of Vertebrate Paleontology and Paleoanthropology, Chinese Academy of Sciences, Beijing 100044, China
[4] College of Earth and Planetary Sciences, University of Chinese Academy of Sciences, Beijing 100049, China

strategy, ontogeny, and behavior of pterosaurs [1]. For example, by studying *H. tianshanensis* 3D embryos, Wang et al. found that newborns could probably move around but not fly, which means that they needed their parents' care [2]. This finding is different from the previous hypothesis that pterosaurs were highly precocial [3]. Furthermore, both male and female pterosaur skulls have crests, and the differences between male and female specimens are mainly in crest size, shape, and robustness [1]. This finding strongly refutes the view that the presence or absence of a cranial crest was a sexually dimorphic characteristic extensive in almost pterosaurs [4]. In addition, the *H. tianshanensis* eggs are mainly composed of calcium phosphate, which rectifies the formal view that calcite is the main component [5].

These significant findings depend on fossil remains, but the fossils have begun weathering since they were transported to Beijing. This weathering includes cracking, powdering, spalling, and disintegration, which seriously endanger the fossil's safety. Li et al. used X-ray fluorescence (XRF), X-ray diffraction (XRD), and other methods to explore the mechanisms of fossil weathering. The results indicated that one of the crucial reasons for fossil corrosion was the high soluble salt content in the fossils and surrounding rock [6, 7]. The high content of soluble salts such as NaCl, $CaCl_2$, $NaNO_3$, $Ca(NO_3)_2$ will generate crystallization pressure and affect the preservation of *H. tianshanensis* fossils and severely threatens the safety of this cultural heritage [6, 8]. When the humidity changes, soluble salts generate massive crystal pressure thus creating high stress and significantly damaging the fossil structure. This dissolution–recrystallization process and resulting pressure was the primary fossil deterioration mechanism [9, 10]. Some researchers have used siloxane-based polymers to increase the mechanical strength and water resistance of fossils based on the poor fossil condition. After a series of examinations, hybrid sol TEOS-TPME-s showed the best performance in protecting Hami fossils [11]. Although consolidation can enhance fossil cohesion, this treatment may increase fossil susceptibility to salt damage, because consolidation may increase the crystallization pressure while filling the porous stone structure and reducing pore radii [12, 13]. Therefore, it is crucial to find a suitable way to reduce soluble salt damage before consolidation.

There are many attempts to mitigate salt damage. One way is using crystallization modifiers, which principle is reducing the pressure of crystallization and/or promoting salt crystallization on the surface (efflorescence) rather than in the pores of materials [14]. However, several reports have shown that the combined use of crystallization modifiers, such as ferrocyanides combined with cellulose poultices could make desalination methods more effective [15]. Nevertheless, using ferrocyanides has a high risk as this can decolor the sample due to UV light [15–17]. Moreover, modifiers are effective only for a specific type of salt [18].

Another control salt decay is reducing the salts content in the affected material. The most widely used method is applying poultices, which is easy to do but the poultice can residue on the heritage surface. Taking clays and cellulose compounds, which were the most frequently used material in conservation for soluble salt extraction for example, these material are easy to remove after the desalination process but are less effective than clay [19]. Meanwhile, clay has better adhesion and higher efficiency than cellulose but is harder to remove, and the residues are always left on the surface of the relics after desalination. Applying Japanese paper as a separator can significantly prevent staining of the substrate, nevertheless, this will still leave very little residues [20] and induce the reduction of extracted salts efficiency [21]. Except for the poultice composition, many variables can affect the treatment outcome, including moisture, temperature, relative humidity, and ventilation conditions, so that the desalination results can be highly variable [22]. Many studies have focused on how poultice composition influences desalination and how to improve desalination effectiveness. Experimental results found that when the poultice had smaller pores than the substrate, the poultice extracted salts efficiently [22], but this does not mean that the smaller pores of the poultice, the better the poultice will be, because the poultice acts as a water reservoir during the wetting phase and should have larger pores than the substrate [23]. Considering both substrate wetting and salt extraction, conservators have found that achieving the most efficient and suitable poultice requires fine-tuning the pore size distribution of the poultice relative to the properties of the substrate during the traditional poultice way [24].

Because the poultice method has many disadvantages, such as limited desalination depth, too many influencing factors, and strict porosity requirements between poultice materials and the desalinized-requiring cultural relics [19], some researchers have focused on electrokinetic techniques to remove soluble salts. The principle of electrokinetic techniques is that the ions migrate towards the electrode of opposite polarity through a porous material when an electric DC field is applied. Consequently, the ionic content in the material is decreased and the ionic content in the vicinity of the electrodes is increased [25]. The Eqs. (1)–(3) are primary electrode reactions transforming the current from carried by electrons in the electrodes to ions in the pore solution.

$$\text{At the anode}: 2H_2O \rightarrow 4H^+ + O_2(g) + 4e^- \quad (1)$$

$$4Cl^- \rightarrow 2Cl_2(g) + 4e^- \quad (2)$$

$$\text{At the cathode}: 4H_2O + 4e^- \rightarrow 4OH^- + H_2(g) \quad (3)$$

This method greatly improves the desalination efficiency but it also has a big problem: the extreme pH value. From step (1) to step (3), the pH increases at the cathode and decreases at the anode. Neutralizing the pH changes to prevent drastic changes is an important part of electrokinetic desalination. Adding calcium carbonate to the poultice is a widely used method to prevent severe pH changes and to guarantee the safety of the desalination samples [26]. The reactions are as follows:

$$CaCO_3 + H^+ \rightarrow Ca^{2+} + HCO_3^- \quad (4)$$

$$HCO_3^- + H^+ \rightarrow CO_2(g) + H_2O \quad (5)$$

Apart from adding $CaCO_3$, using a buffer solution is also an excellent way to stabilize pH values at around 7. A previous study chose a solution of 0.2 M sodium citrate and 0.2 M citric acid buffered to pH 6 as electrolytes, and the needed buffering solution concentration is dependent on applied current and duration following the Eqs. (1)–(3) [26–28]. Buffer systems formed by a localized buffer electrolyte sponge and $CaCO_3$ added to the poultices have shown their effectiveness [29]. The electrokinetic technique proved effective on desalination in laboratory studies and was applied to artifacts for removing the soluble salts in situ [28, 30, 31]. This method has developed in an increased interest among researchers because it has shown promising results and is recognized as an efficient way of removing salts [32].

Overall, previous studies have shown that there are many ways against salt damage for stone relics. Nevertheless, little research has been focused on the desalination of fossils and their surrounding rocks. In view of the high scientific value and the severe weathered station, it is essential to have some treatment for salt weathering. Since using crystallization modifiers has many limitations, we preferred to reduce the ionic content. Considering the large size of the Hami pterosaur (a 3.28 m^2 sandstone block), immersion baths are not a good choice because this method only valid for small samples. Here, we applied a combination of techniques such as Mercury Intrusion Porosimetry (MIP), Scanning Electron Microscopy and Energy Dispersive Spectroscopy (SEM-EDS), Ion Chromatography (IC) and Reflectance Spectrophotometer to perform desalination tests on small blocks collected from the larger specimen. Thus, this work focuses on assessing the effectiveness and risks of different electrokinetic desalination interventions.

Materials and methods

Rocks used

In this work, the sample is from *H. tianshanensis* fossils, which were collected from the Institute of Vertebrate Paleontology and Paleoanthropology (IVPP). The rock was collected from the fossil under preparation. The pterosaur fossils were originally collected at the Turpan-Hami Basin, Xinjiang Uygur Autonomous Region, northwestern China, and almost specimens were found in the tempestite interlayers. The fossil-surrounding rocks are a sandstone mixture of grayish-white sandstone and brown mudstone breccia (Fig. 1A). The pterosaur fossil and its surrounding rocks have begun weathering since they were transported to Beijing. The surrounding rocks are disintegration and pulverization, causing pterosaur bones and eggs to fall off due to lack of support from surrounding rock (Fig. 1B).

Studies on fossil bone and matrix of Hami pterosaurs were previously presented by Li et al. [6, 7]. The characterization of the matrix of pterosaur fossils and bones was carried out by X-ray diffraction analysis (XRD), as shown in Fig. 1D: the sandstone mainly consists of quartz (43.2 wt%), feldspar (37.4%), carbonated (7.4 wt%), clay mineral (12%). Hence, the fossil surrounding rocks can be assumed as clay-rich (i.e., clay $\geq$ 5 wt%) sandstone [33]. Notable, the clays are mainly montmorillonite (8 wt%), and its characteristic of water swelling and drying shrinkage during humidity changes will cause damage in the connection between particles. Likewise, the clay mineral leads to grain-by-grain detachment for fossils surrounding rocks of Hami pterosaur when the humility cycling [7]. Apart from the clay mineral, the soluble salts such as halite, also lead to the granular disintegration of the fossil-surrounding rocks under the fluctuations between high a low relative humidity [7].

This study involved one big fossil-surrounding rocks for the experiment. The rocks were segmented with a chisel and saw by hand. Wet sawing was not used for segmentation because water to the stone would lead to salts redistribution. Figure 2 shows the original rocks and their segmentation. The rock was segmented into 5 segments. One segment (No. 5) was used as the reference stone to detect the distribution of the initial salt among different areas and depths. Two segments were used for electrochemical way (with paper pulp/ CKS 121).

Materials

The cellulosic powder used to prepare for the desalination poultice was Arbocel® BC 1000 (fiber length

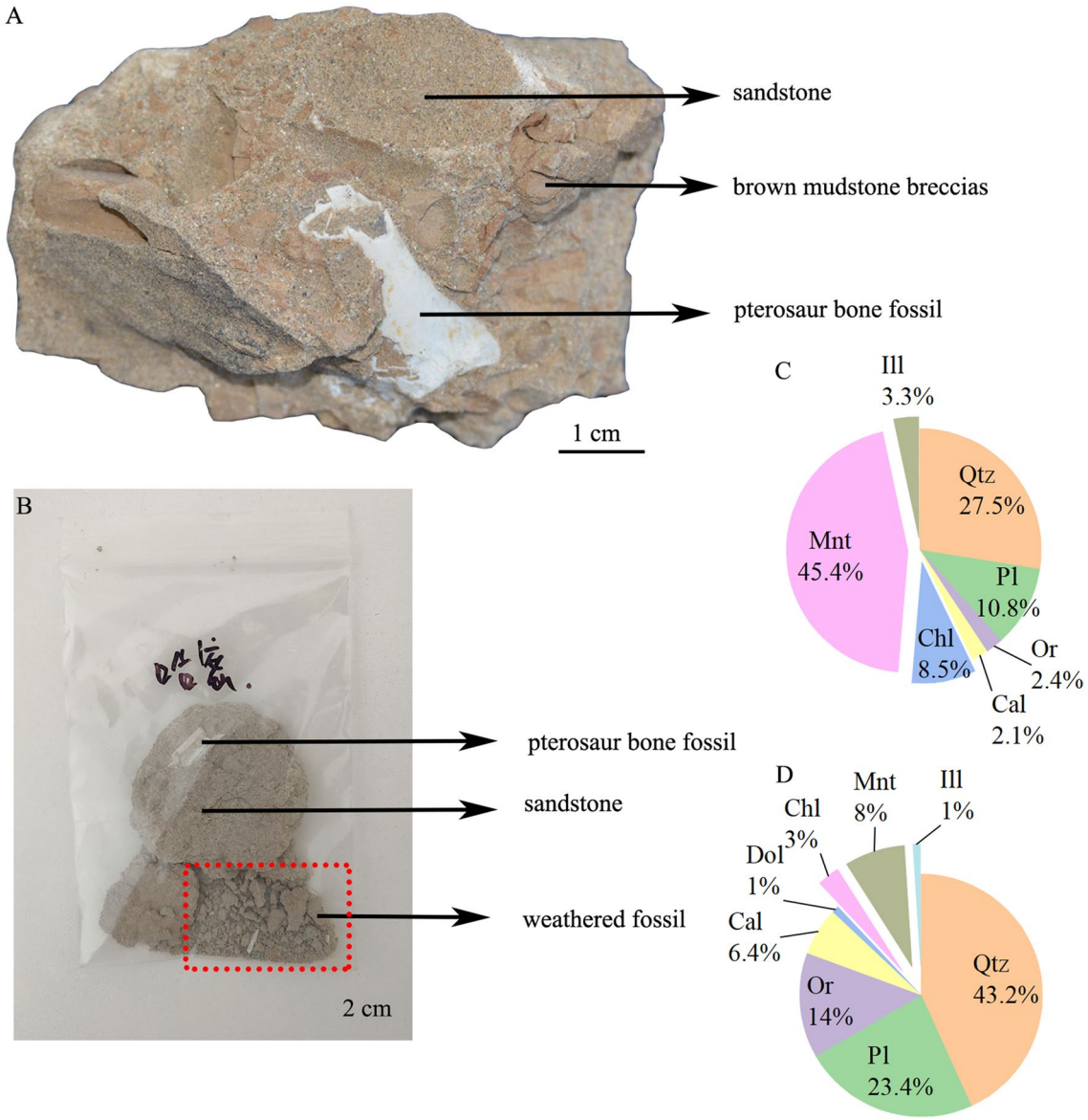

Fig. 1 Pterosaur fossil bones encased in sandstone matrix, and their mineral composition. **A** Pterosaur fossil and fossil-surrounding rocks. The fossils are embedded in sandstone with brown boulder clay. The hollow pterosaur bone fossil is thin and fragile. When the surrounding rock is pulverized and exfoliated, the fossil begins to crack and exfoliate because of a loss of mechanical support. **B** the weathered fossil. The specimens were collected in the field and was put into the sample bag. When the fossil transported indoors, the surrounding rock was powdery and some bones were broken. **C** The mineral composition of mudstone breccias (wt%). **D** The mineral composition of sandstone (wt%). Pie charts (**C–D**) are based on the XRD results from Li et al. [7]

700 μm). The silica sand (0.55–1 mm) and kaolin were purchased from Macklin Chemical Co., Ltd. The paper pulp for desalination was Bioline® desalinated poultice[1], which has been used in conservation projects such as the Dayan Pagoda conservation project before. This poultice is viscous fibrous slurry and cream colored. The citric acid–sodium dihydrogen phosphate (pH 7.0) was purchased from ROBY Tech. Co., Ltd. The citric acid–sodium dihydrogen phosphate (pH 6.0) was purchased from Nanjing Keygen Biotech. Co., Ltd.

[1] The poultice is from Zhejiang Desaibao Building Materials Technology Co., Ltd, China. More details about this poultice can be seen in website: https://www.dsbioline.com/.

Fig. 2 Original fossil-surrounding rock and its segments. **A** Original fossil-surrounding rock (scale bar: 5 cm); **B** Segment No. 1 (scale bar: 2 cm); **C** Segment No. 2 (scale bar: 3 cm); **D** Segment No. 3 (scale bar: 3 cm); **E** Segment No. 4 (scale bar: 3 cm); **F** Segment No. 5 (scale bar: 3 cm)

Table 1 Material parameters of the applied poultice mixtures in electrochemical method

Poultice type	Cathode		Anode	
	Composition (w/w)	Water content (weight water/weight dry poultice)	Composition (w/w)	Water content (weight water/weight dry poultice)
CKS121	Cellulose: kaolin: sand = 1:2:1	0.8	Cellulose: kaolin: sand: $CaCO_3$ = 1:2:1:1	0.8
Bioline® desalinated poultice	Paper pulp	/	Paper pulp: $CaCO_3$ = 4:1	/

Desalination experiments setup

Two kinds of poultices were employed, about 10 mm thick, as the reservoirs for the ions extracted from the rocks. One was the Bioline® desalinated poultice, a Chinese paper pulp which has been used in the Dayan Pagoda conservation project previously. The other was CKS121, which has been used in many laboratory studies [34]. The specific composition was a mixture made of cellulose: kaolin: sand = 1:2:1 (w/w). The water content was 0.8 (weight of water/weight of dry poultice material). In addition, the poultice at anode added $CaCO_3$ to buffer the acid produced by electrolyzed water. Specific experimental conditions are shown in Tables 1 and 2.

Sponges, about 2 mm thick, were soaked with the electrolyte to avoid extreme pH, and then the sponges were put between the graphite electrode and the poultices. At the anode, hydrogen ions are produced during electrolysis, so a buffer solution of 0.2 M citric acid/sodium citrate with pH = 7 was applied. For the cathode, OH^- ions are produced, so a buffer solution of 0.2 M citric acid/sodium

Table 2 Experimental conditions for the desalination experiments

Poultice used	Stone number (size)[a]	Initial current (mA)[b]	Duration (days)	Remarks
paper pulp	No. 1 (5/6/6)[a]	10	15	Poultice replaced every 3 days
CKS 121	No. 4 (6/7/7)	10	15	Poultice replaced every 3 days

[a] Numbers within the parentheses mean the samples size. For example, No. 1 (5/6/6) means that this stone segment (No. 1) is about 5 cm long, 6 cm thick and 6 cm high

[b] The DC power supply was set to supply a constant current of 10 mA. Thus, the initial current was 10 mA. Since the increasing resistance during the experiments, the current could no longer maintain at 10 mA and began to decrease at a constant voltage of 20 V

citrate with pH = 6 was applied. The electrode material used in this experiment was graphite (2-mm thick) because of its efficiency and economy. PVC film wrapped the whole system to avoid evaporation. The elements used in the assembly are shown in Fig. 3A.

The direct current (DC) paper pulp and CKS121 desalination experiments were connected in series. The DC power supply was set to supply a current of 10 mA and when this condition could not be sustained the system was run at constant voltage (20 V). When we switched on the power supply, the current was 10 mA, and the applied potential voltage was less than 20 V. Because of the increasing resistance during the experiments, the voltage was increased gradually up to the 20 V (the setting

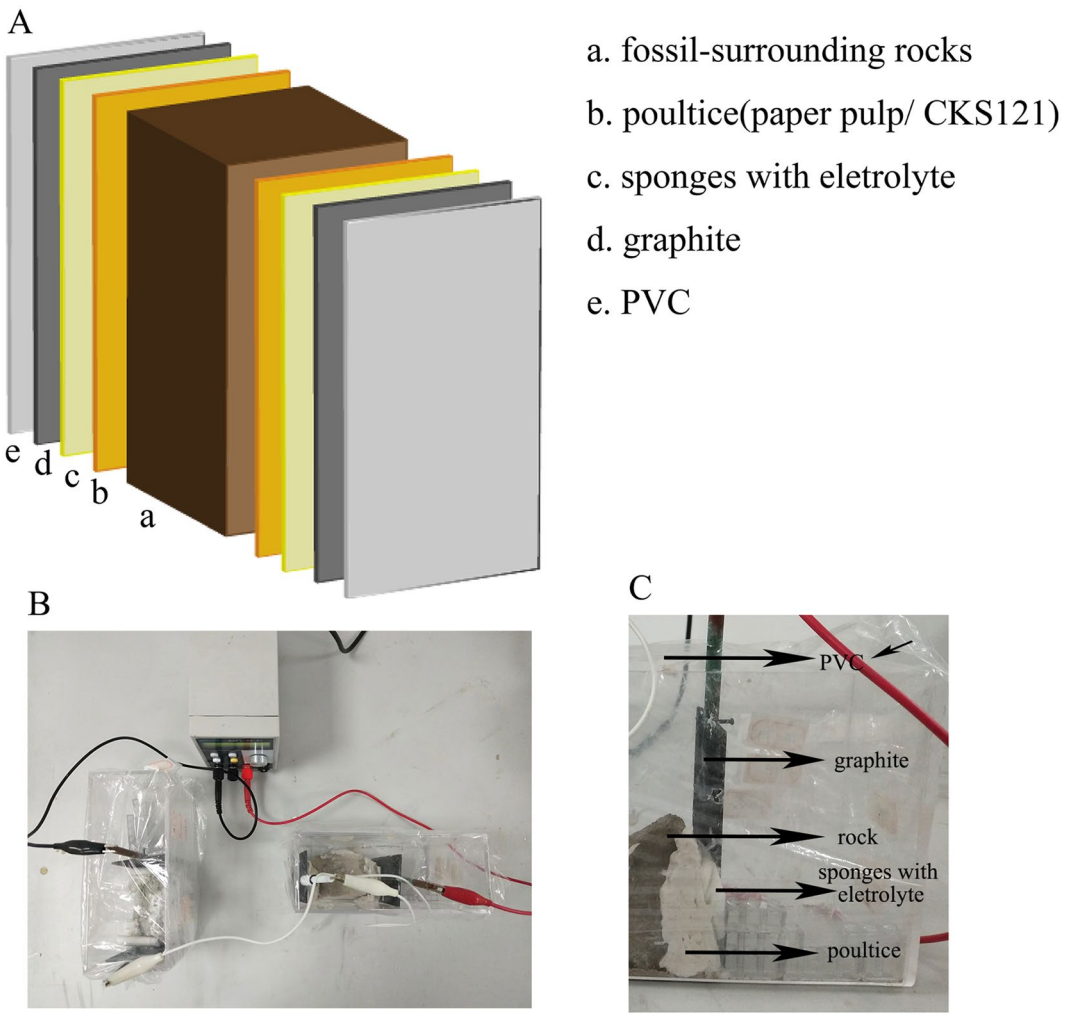

Fig. 3 Desalination experiment setup. **A** Schematic draw of specimen assembly and composition of various elements for electrokinetic desalination. Moreover, the fossil-surrounding rocks used in the actual desalination experiments were kind of irregularly (not cubic). **B** The real picture of electrokinetic desalination experiment. **C** The enlargement for the electrokinetic desalination using paper pulp

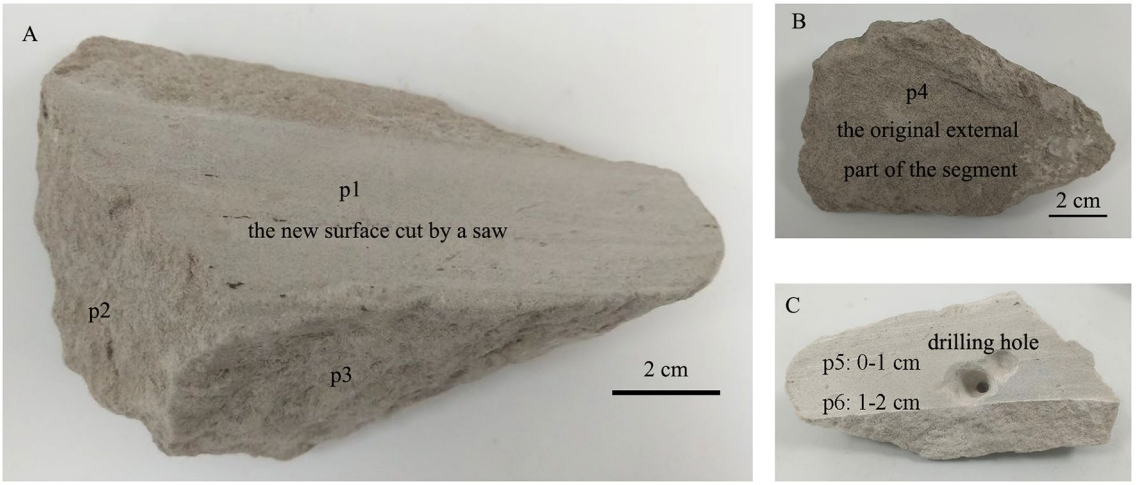

Fig. 4 The location of powder sample for IC

value) and the current was maintained at 10 mA during this time. When the maximum of 20 V was reached, the current could no longer keep at the same level at 10 mA and the current began to decrease at a constant voltage of 20 V. Every 72 h, the poultices and sponges were replaced. This process also lasted 15 days. The laboratory experiment setup for the electrokinetic desalination is shown in Fig. 3.

Analytical methods

Microstructural characteristics of poultices and substrates

In order to have a better understanding of the characteristics of poultices and substrates, mercury intrusion porosimetry (MIP) and SEM were used to detect the pore size distribution. Moreover, SEM-EDS was used to detect the chemical composition of salts in the fossil matrix.

(1) Mercury intrusion porosimetry

MIP was used to determine the pore size distribution of the surrounding rocks (substrate) and poultices (CKS121 and Bioline®). Testing samples were put in a crucible in a muffle furnace under 105 °C for 12 h to obtain dry samples for the MIP test. The test was conducted using an AutoPore IV 9500 (Micromeritics Instrument Corporation). The mercury contact angle was 130°.

(2) SEM-EDS analysis

The poultices and fossil-surrounding rocks were dried in the muffle furnace and coated with gold before SEM-EDS analysis. The microstructure and chemical composition of samples were examined on a SEM-EDS (Zeiss E.V.O. 25 SEM couple with Oxford INCA energy-dispersive X-ray spectroscope Carl–Zeiss, Germany) with 20 kV voltage.

Treatment evaluation

After desalination experiments, the rocks were naturally dried. IC was used to obtain the ion contents for evaluating the efficiency of different desalination methods. And the global color change was measured to evaluate the risk of the intervention.

(1) Soluble salt content

Six powder samples of segment No. 5 were taken to detect the initial ion content variations over the object (Fig. 4). Four powder samples were taken by scraping the surface with a scalpel: powder samples No. p2, p3, and p4 were from the original external part of the segment, powder sample No. p1 was from the new surface cut by a saw. Another two powder samples were taken by drilling: powder samples No. p5 and p6 were collected across assembly levels of: and 1–2 cm, respectively, starting from the saw-cut new surface.

For each fossil-surrounding rock (before segmentation), one powder sample was collected by scraping the surface with a scalpel in order to detect the initial ion content. After desalination experiments, each desalinated sample was cut through the middle and then powder from the interior and surface areas was scraped to study the difference in the soluble salt content of the desalted block. In summary, one powder samples for initial salts content and four powder samples for salts content after desalination. The surface powder was collected from no poultice-covered areas.

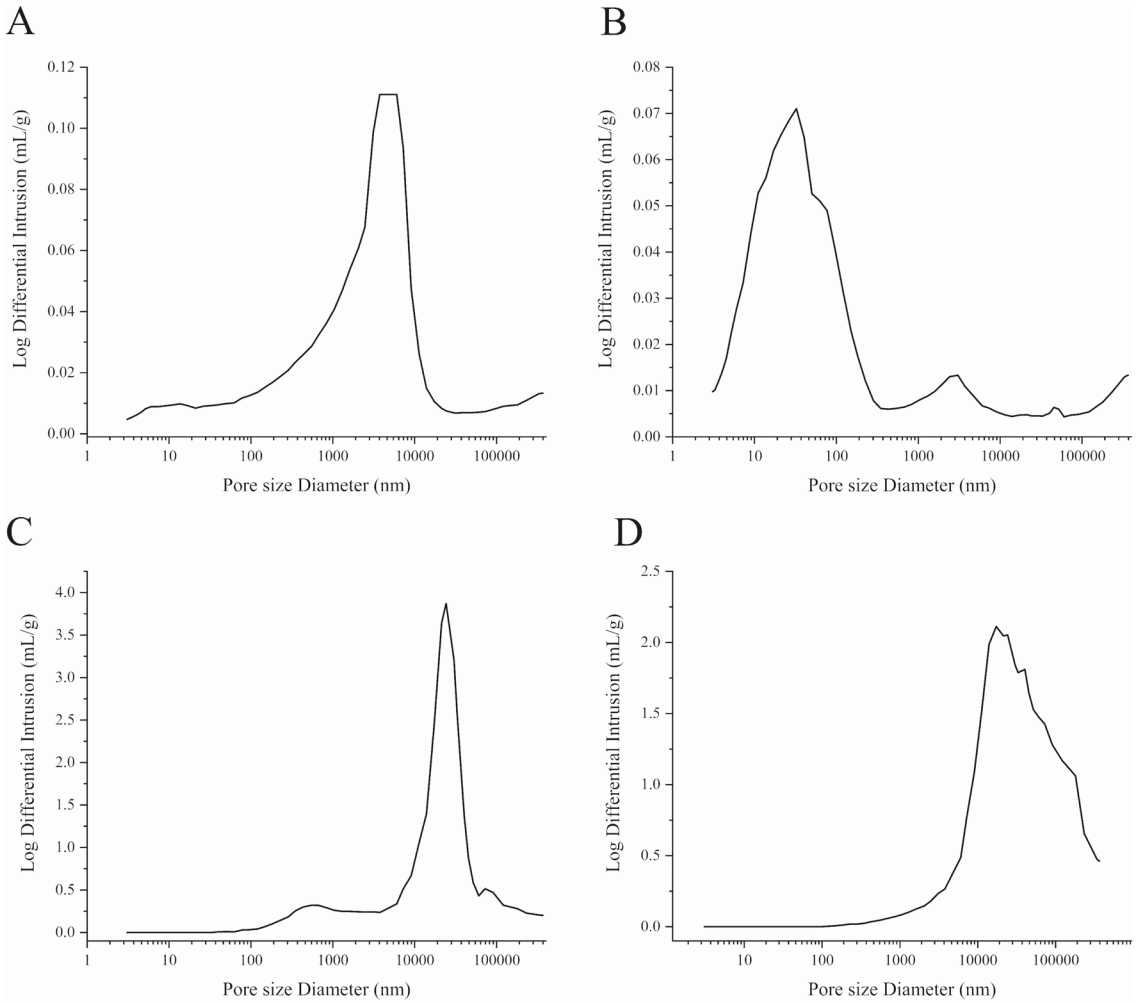

Fig. 5 Pore size distribution of substrate and poultices. **A** Fossil-surrounding rocks (sandstone). **B** Fossil-surrounding rocks (sandstone with boulder clay). **C** CKS121 poultice. **D** Bioline® desalinated poultice

Soluble salts were identified via the following steps: 0.1 g of powdered sample was added to a 25 ml volumetric flask, and the quantity was fixed with ultrapure water. The suspension was agitated for 72 h and then filtered through 0.22-μm mesh filters. In the aqueous extract, anions (Cl^-, SO_4^{2-}, and NO_3^-) and cations (Na^+, K^+, Mg^{2+}, and Ca^{2+}) were determined by IC using the HIC-10 A super IC (Shimadzu Corporation, Japan).

(2) Color change

After desalination, the sample was cut through the middle to determine whether the color of surface and interior of the sample have changed. The specimen reflectance spectra were measured by a reflectance spectrophotometer (X-Rite VS450 spectrophotometer, USA). Measurement conditions were as follows: the optical geometry 45/0°, 45° gloss, spectral range 400–700 nm; spectral interval 10 nm, diffused viewing with a 6.0-mm aperture diameter. The color of each sample was measured using color measurement software (X-Rite Color Master, USA).

Results and discussion

Characterization of rocks and poultices

Fossil surrounding rock

(1) Pore size distribution

Since fossil-surrounding rocks are the sandstone mixture of grayish-white sandstones and brown mudstone breccias (Fig. 1A), the sandstone and the mudstone breccia were detected by MIP separately. The main range for the pore size distribution in the sandstone

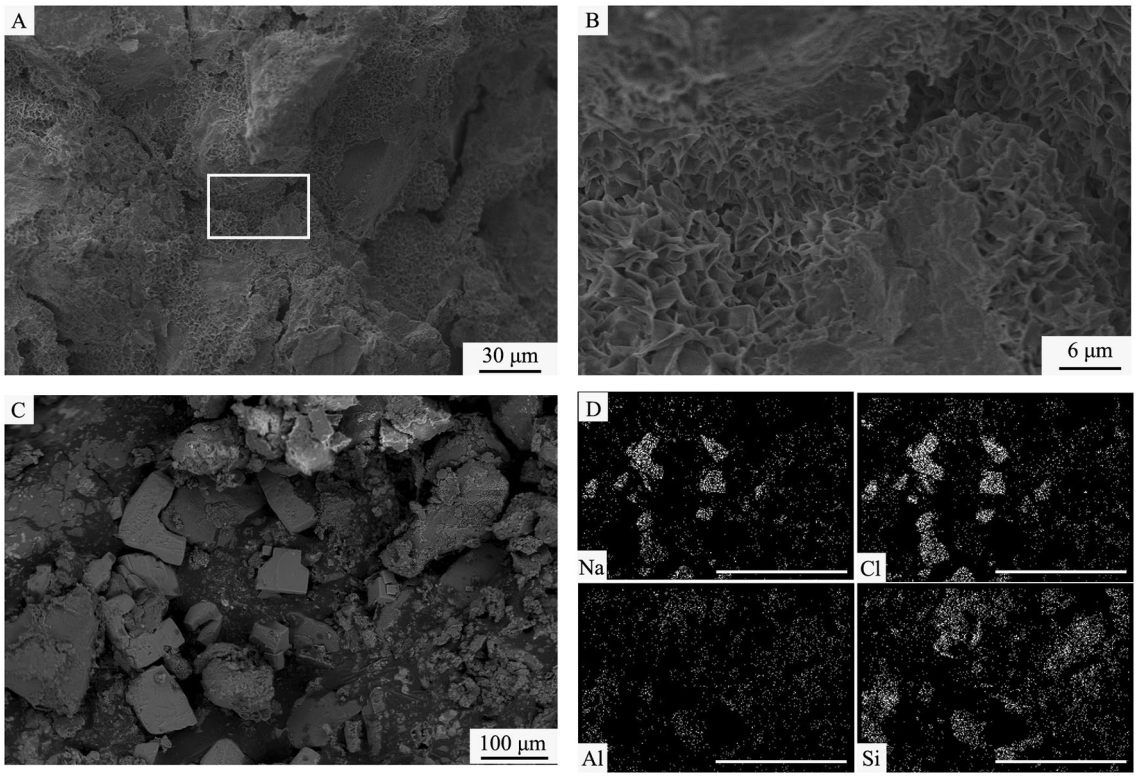

Fig. 6 SEM images and element mapping of fossil surrounding rocks. **A** Secondary electron images of fossil-surrounding rocks, showing the montmorillonite coating (C-Mnt) attached to the grain surface; **B** Secondary electron images of the enlargement for detail of the white box in fig. A showing flat shaped crystals, like curled leaves piled-up, of montmorillonite; **C** Backscattered electron (BSE) image of crystals in the fossil-surrounding rocks; **D** The element mapping of fig C, showing the major presence of Na and Cl in the fossil-surrounding rocks, revealing that the salt crystals are halite. Bar = 400 μm

part is narrower (Fig. 5A), but the pores are larger (1000–10,000 nm), while the range for the sandstone with boulder clay is broader (Fig. 5B), but the pores are smaller (10–100 nm).

Figure 6 presents the microstructural characteristics of the fossil surrounding rocks. Under the SEM it can be observed angular grains of quartz and feldspar surrounded by clay minerals (Fig. 6A). Clay minerals are flat in shape, like curled leaves piled up (Fig. 6B), which is typical of montmorillonite [35]. In addition to the distribution characteristics of clay minerals, the chemical composition and distribution of salts in the sandstone can also be observed by SEM-EDS. As shown in Fig. 6D, the element mappings show the correlation of sodium with chlorine, indicating the cubic crystals shown in Fig. 6C are halite (NaCl). Furthermore, cubic crystals are the most common form of halite.

The SEM results indicated that the clay mineral and salts can be cementation in sandstone, which is consistent with the previous study [7]. The main water-soluble salts found in fossil-surrounding rocks are halite.

(2) Salts in fossil surrounding rocks before desalination

The reference stone (the segment No. 5) was used to detect the distribution of the initial salt among different areas and depths. As shown in Table 3, the initial average salt content was 13,020 ± 1011 μg/g. The low deviation indicates the salt concentrations are similar among different depths. Nevertheless, considering the fossil surrounding rocks are non-homogeneous natural materials, the ion content cannot be the same in different place despite the stones are of the same type and were taken from the same fossil.

The Austrian standard ÖNORM B 3355-1 is the only accessible threshold values to evaluate the salt concentrations has risk or not [36]. The limits are: (critical limit-limit for no risk): Cl^- (1000 ~ 300 mg/kg), NO_3^- (1500 ~ 500 mg/kg), SO_4^{2-} (2500 ~ 1000 mg/kg). All the measured Cl^- concentrations is above 4000 μg/g and NO_3^- concentrations is above 1500 μg/g, which indicates that the Cl^- and NO_3^- concentration are high compared to the threshold values. Moreover, the SO_4^{2-} concentrations were in the range classified no risk. In summary,

Table 3 The ion content of the segment No. 5 (μg/g)

Number[a]	Na^+	K^+	Ca^{2+}	Cl^-	NO_3^-	SO_4^{2-}	In total
p1	3003	159	3060	5417	1719	138	13,498
p2	2935	224	2884	5034	1729	212	13,018
p3	3224	229	3057	5826	1938	210	14,483
p4	2544	232	2639	4812	1827	139	12,193
p5	2045	238	3218	4440	1532	141	11,615
p6	2563	374	3657	4803	1807	112	13,316
Average	2719	243	3086	5055	1759	159	13,020
Deviation	422	71	342	495	136	42	1011

[a] Powder sample No. p1 from the new surface cut by a saw, powder samples No. p2, p3, and p4 from the original external part of the segment (Fig. 4). Another two powder samples were taken by drilling: powder samples No. p5 and p6 were collected across assembly levels of 0–1 cm and 1–2 cm, respectively, starting from the saw-cut new surface (Fig. 4)

these results show that the difference of ion contents among different parts are not significant despite the ion contents of fossil is non-homogeneous. Therefore, here we used the surface ion content approximately reflect ion content of the whole sample.

Poultice

In view of the sample for MIP and SEM tests need to be dry, the poultices are both after oven drying. Although the dry condition cannot completely represent the moist situation that comes into existence during desalination, these results can reflect the pore distribution to some extent. Lubelli and van Hees believed that there is no significant differences between the pore size of the dry poultice and the pore size of the poultice when it starts working by advection in most of the cases (cellulose, kaolin and sand based poultices) [24]. Hence, MIP has been used for measuring the pore size distribution of poultices in many researchers [24, 37–39].

As shown in Fig. 5, there is a great difference in pore size distribution between CKS121 and paper pulp. The main range for pore size in CKS121 is 100–100,000 nm, and there is a narrow peak at 12,000 nm. CKS121 also has a small peak at 400 nm because the kaolin partially fills up the interstitial porosity of the cellulose. For the Bioline® desalinated poultice, there is a broad size distribution (10,000–100,000 nm), and the peak is at 11,000 nm.

The pore size distributions can be divided into three categories referred to Kröner et al. [21]: fine-size pores (< 1 μm), medium-size pores (1–75 μm), and large-size pores (> 75 μm). CKS 121 has some fine pores, a great number of medium pores, and some coarse pores, while Bioline® desalinated poultice has a few fine-size pores, a large amount medium-size pores, and many of large-size pores.

Apart from MIP, SEM is another method for describing the pore structures of porous material. For the CKS121, the large pores are located around the sand grains (Fig. 7A); the spaces between the cellulose fibers are filled with kaolin (Fig. 7B), which adheres to the cellulose fibers (Fig. 7C). This leads to a reduction in the number of large pores (> 50,000 nm) and creates more small pores (400–1000 nm). For the Bioline® desalinated poultice (Fig. 7D), the fibers of different shapes and lengths are snarled up. The network of cellulose fibers is unfastened and disordered. The number of large pores is significantly greater than in the CKS121, which is consistent with the MIP results.

Desalination tests

Ion contents after electrokinetic desalination

Table 4 shows the fossil's soluble salt contents before and after electrokinetic desalination treatment. The reduction in surface salt content was 71.60% when using CKS121 with the DC applied method. When using paper pulp, the surface salt reduction was 70.75% with DC. In addition, the data in Table 4 reveal a noticeable difference value in the soluble salt content between the surface and interior area of the fossil-surrounding rocks. The surface area has a higher salt content. A possible explanation for this is that the desalinated poultice has a low absorbing ability, and ions aggregate at the surface.

Table 4 provides the summary statistics for salt reduction, and Fig. 8 shows the characteristics of each ion when using the electrokinetic desalination method. It shows that most ions (Na^+, K^+, Ca^{2+}, Cl^-) of the interior ions were lower than surface ions. This may be explained by the low absorbing ability of poultice. In the interior, ions can quickly move to the surface following the DC field, but they cannot be immediately absorbed by the poultice thus causing the accumulation of ions on the surface.

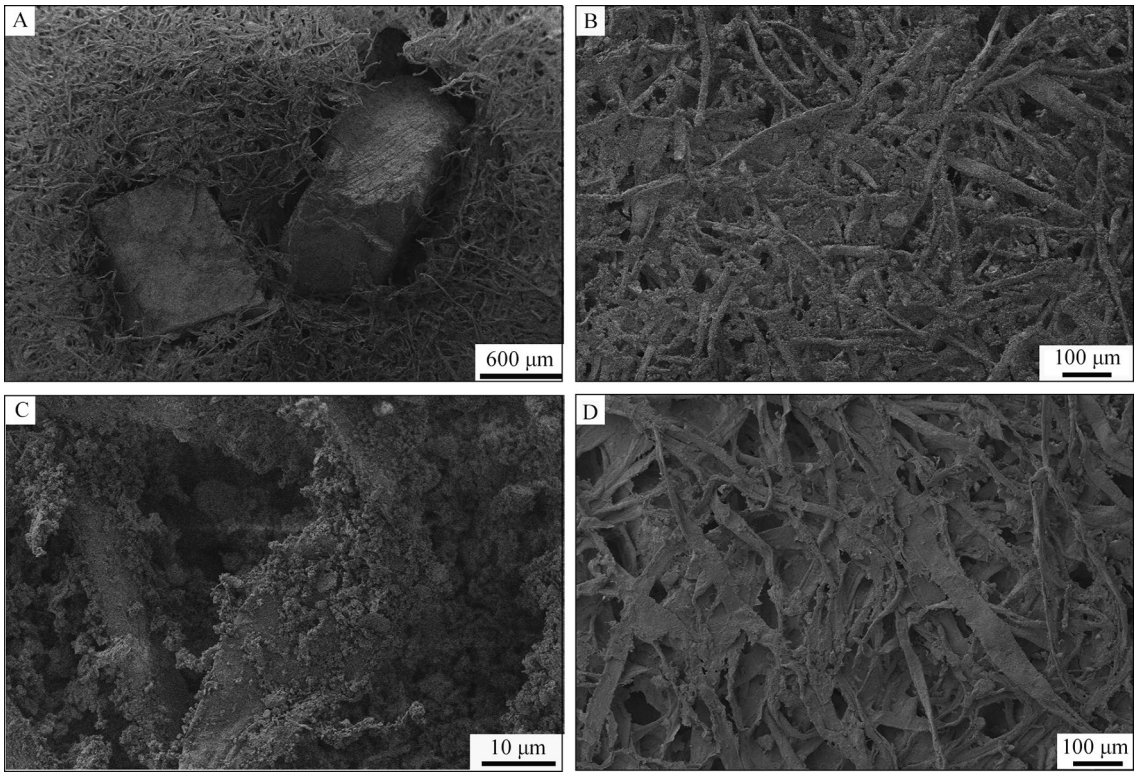

Fig. 7 Secondary electron images of poultices. **A–C** CKS121poultice. **D** Bioline® desalinated poultice

Table 4 Total soluble salt content of samples before and after desalination treatment. The effectiveness of the removal of the salts in percentage is also shown

	All soluble salts content (μg/g)	Efficiency (%)
Initial	13,943	\
MS	3960	71.60
MI	2741	80.34
PS	4078	70.75
PI	3028	78.28

MS rock surface when using CKS121 poultice, *MI* rock interior when using CKS121 poultice, *PS* rock surface when using Bioline® desalinated poultice, *PI* rock interior when using Bioline® desalinated poultice

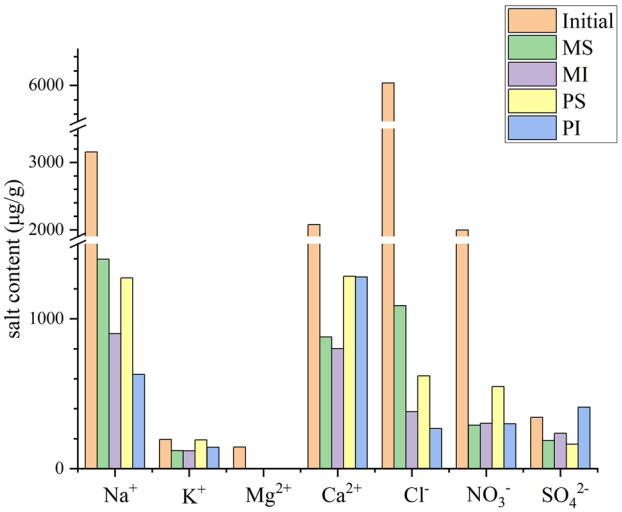

Fig. 8 The soluble salt content in initial rocks and after desalination using the DC method. *MS* rock surface using CKS121 poultice, *MI* rock interior using CKS121 poultice, *PS* rock surface using Bioline® desalinated poultice, *PI* rock interior using Bioline® desalinated poultice

In addition, the SO_4^{2-} removal efficiency was the lowest. For both CKS121 and paper pulp, the SO_4^{2-} showed no obvious difference from the untreated sample. Similar results also appeared in other researchers' works [40–42]. The lowest SO_4^{2-} removal efficiency could be related, theoretically, to sulfate's low ionic mobility ($^1/_2SO_4^{2-}$ 4.2×10^{-8} $m^2V^{-1}s^{-1}$), while compared with NO^{3-} (7.4×10^{-8} $m^2V^{-1}s^{-1}$), Cl^- (7.9×10^{-8} $m^2V^{-1}s^{-1}$),

Table 5 Colorimetric differences (ΔL*, Δa*, Δb*) and total color difference (ΔE*ab)

	EMI	EMS	EPI	EPS
ΔL*	5.95	14.03	−1.28	6.91
Δa*	−0.05	−2.26	−0.44	−0.65
Δb*	0.12	−8.31	0.26	−1.52
ΔE*ab	5.95	16.46	1.38	7.10
Risk	H	H	L	H

Na^+(5.19×10^{-8} $m^2V^{-1}s^{-1}$), K^+ (7.62×10^{-8} $m^2V^{-1}s^{-1}$), Ca^{2+} (6.17×10^{-8} $m^2V^{-1}s^{-1}$), and Mg^{2+} (5.5×10^{-8} $m^2V^{-1}s^{-1}$) [43, 44]. Because SO_4^{2-} has the lowest ionic mobility, only surface SO_4^{2-} ions were adsorbed, and the inner SO_4^{2-} concentration did not change obviously. From the study by Ottosen et al., the removal rate of SO_4^{2-} would increase significantly only when the content of Cl^- and NO_3^- were very low [41]. Another possible explanation for this is that sulfate and calcium ions in the fossil-surrounding rocks precipitate gypsum [45], which reduces the efficiency of SO_4^{2-} reduction. The interior SO_4^{2-} content is a little bit higher than the untreated sample for paper pulp, partly because the salt distribution in the untreated sample is inconsistent. When detecting the initial soluble salt content, powders were only scraped from the surface, so accurate interior salt content was not detected. The transport mechanism and mutual influence of mixed salts on electrochemical desalination need further research.

From the above results and discussion, it can be concluded that using CKS121 is a little bit effective than paper pulp. This can be explained by the different properties of poultices. First, the pore size distribution between the two poultices is different. As shown in Fig. 5, the rocks have a large number of medium-size pores (1–75 μm), and the CKS 121 has more fine pores (< 1 μm) than Bioline® desalinated poultice. The large pores of poultice (compare with stone) ensure suitable wetting of material to be desalted, while the small pores ensure the advection from stone to poultice. In other words, a significant quantity of the poultice pores are smaller than those of the substrate, the salt extraction can be proceed efficiently [22]. Since CKS121 poultice has more small pores than paper pulp (Bioline® desalinated poultice), CKS 121 will have a better desalination ability because of the advection. In addition, Kaolin is added to CKS121 poultice, and this clay mineral has high adsorption because of the large specific surface area, chemical and mechanical stability, layered structure, high cation exchange capacity [46].

The appearance changed

There was some residual material left on the surface, which changes the color (Fig. 9). Spectrophotometer can measure the color change quantificationally and ΔL was a parameter to evaluate the color difference change. According to Table 5, the ΔL* value of the surface is positive and exceptionally high, which means that, after desalination, the rocks are whiter than before treatment. This is likely related to powder residue, like kaolin, on the surface. The Δb* value of EMS is negative, which means that after desalination, the rocks were bluer than before treatment. In summary, electrokinetic methods have a high risk of surface color change. This considerable color change is a negative result of desalination that needs to be improved. One solution is using Japanese paper in the future work to wrap the samples in order to avoid poultice residue on the fossil surface.

Risk assessment with reference to Rodrigues and Grossi (2007) [47]. *H* high risk (ΔE*ab > 5), *M* medium risk (3 < ΔE*ab < 5), and *L* low risk (ΔE*ab < 3). *EMI* represents rock interior when using CKS121 with DC, *EMS* represents rock surface when using CKS121 with DC, *EPI* represents rock interior when using paper pulp with DC, *EPS* represents rock surface when using paper pulp with DC

Except for color changes, fossil appearance also changed due to cracking (Fig. 9), which can be explained by the montmorillonite swelling-induced stresses. The SEM results shows that montmorillonite plays a role in cementation (Fig. 6A), which make the fossil surrounding rocks are susceptible to moisture. The swelling of montmorillonite causes a large volume change with the moisture content increasing during desalination, and it also shrinks as it dries out [48]. As water is absorbed, the mechanical stresses generated by the swelling clay minerals may lead to the cracks. In view of the fact that water dissolving the salts is the crucial part in desalination (only dissolved salt ions can travel from the substrate back into the poultice), some pretreatments to improve the water-resistant for fossil surrounding rocks should be considered. Pre-consolidation can be a promising way to deal with the intense sand disaggregation material during desalination [49, 50]. Apart from applying (brushing or spraying, etc.) chemical consolidants on the surface to improve the cohesion between the mineral grains, the electro-precipitation is a promising way. Theoretically, electrokinetic way can realize desalination and consolidation in one electrochemical device. The ions for precursors of the inorganic compound transport in stone and precipitated, while the ions present in the stone are transported out [51]. Hence, electrokinetic treatment may be

Fig. 9 The contrast between initial and desalinated rocks used the DC method. **A** Initial surrounding rocks. **B** Desalinated rock using paper pulp, **C** Initial surrounding rocks. **D** Desalinated rock using CKS121

an excellent way to protect the Hami pterosaur fossil, because the electrokinetic desalination has a high salt removal efficiency in this experiment and electrochemical synthesis has been used in consolidation for deteriorated materials [51–53].

According to previous studies, extreme pH is another problem limiting the application of electrochemical desalination. Testo 206 was used to detect the pH of the poultices after use; the results indicated that the pH for all of the poultices was within the range of 7–9, which suggests that adding calcium carbonate and using a buffer is an excellent way to avoid extreme pH.

In summary, the electrokinetic desalination method has a high salt removal efficiency. An obvious advantage of this method is saving poultice material. Poultice with electrodes only placed in opposite two surfaces, and this is enough to let the electric field distribute into fossil rocks. Hence, poultice need not cover all the surfaces, whereas poulticing usually does. This can reduce the amount of poultice using, which is economy and avoid waste. In addition, the poultice can be placed around the fragile parts (fossil bones) at in situ desalination. More importantly, electrokinetic treatment can combine the desalination and consolidation, which is a promising way to desalinate for the water-sensitive fragile material. Nonetheless, electro-desalination is an under-development method and many problems need to be solved. One biggest problem is that the electrode and poultice as well as the poultice and rocks cannot maintain a good contact so that manual interference is necessary during the electro-desalination. A similar phenomenon was also reported in the research of Ottosen and Christensen [30], and it was that the combination of decreased poultice volume and gas evolution caused the poor contact. Further research should be undertaken to solve this problem.

Conclusion

This work evaluated the electrokinetic desalination performance for the Hami pterosaur fossils and the surrounding rock, and two types of poultices employed including paper pulp from Bioline® and CKS121. The electrokinetic method with CKS121 has a little bit high desalination efficiency than Bioline® poultice. The differences can be partly explained by different properties of poultices, such as the pore size distribution. Furthermore, the desalination efficiency of the surface is a bit lower than the interior. In addition, electrokinetic method has the high removal efficiency of Na^+ NO_3^- and Cl^-. However, the procedure was not as effective for removing SO_4^{2-}, and the low removal efficiency can be partly explained the sulfate's low ionic mobility and the precipitation of gypsum. Although electrokinetic desalination has a high salt removal efficiency, the high risk of surface color change needs to be improved. Moreover, our study also documented the appearance of cracks in the surrounding rock after electrokinetic desalination. The cracks can be associated with stresses induced by swelling of the montmorillonite due to increased moisture during desalination. Further studies should aim to improve the electrochemical method of clay-rich fossil-surrounding rocks. Pre-consolidation, especially for the electro-chemical method may solve the cracking problem for the clay-rich sandstone desalination. This study focused on the desalination of fossils and the surrounding rock, whereas the findings can be relevant for stone cultural relics, especially for the clay-bearing sandstone.

Acknowledgements
The authors are indebted to the Chinese Academy of Cultural Heritage conservator CHEN Yue, DU Jing, HU Fengdan for their assistance in ion chromatography analyses. We express our gratitude to JIANG Shunxing, JIN Xun, ZHOU Hongjiao, XIANG Long, LI Yang, ZHANG Xinjun, CHEN He, ZHU Xufeng, from IVPP (the Institute of Vertebrate Paleontology and Paleoanthropology, Beijing, China), for their help in the fieldwork, laboratory tests, and helpful advice.

Author contributions
Conceptualization, YL and WL; methodology, YL; software, YL; validation, YL, YY, WL and XW; formal analysis, YL; investigation, YL; resources, WL and XW; data curation, YL and WL; writing-original draft preparation, YL; writing-review and editing, YL, YY, WL and XW; visualization, YL; supervision, YL, YY, WL and XW; project administration, WL and XW; funding acquisition, YL,WL and XW. All authors have read and agreed to the published version of the manuscript.

Funding
This work was supported by the National Social Science Fund of China under Grant [number 20VJXG018], the National Natural Science Foundation under Grant [numbers 42288201], the Beijing Social Science Found Project (No. 21DTR046), the Fundamental Research Funds for the Central Universities and the Hami City Government Cooperation Project, Innovation project, Institute of Archaeology, Chinese Academy of Social Sciences (2021KGYJ023).

Availability of data and materials
The data is available on reasonable request.

Declarations

Ethics approval and consent to participate
Not applicable.

Consent for publication
Not applicable.

Competing interests
The authors declare no competing interests.

Received: 17 August 2023 Accepted: 23 September 2023
Published online: 03 November 2023

References

1. Wang X, Kellner AA, Jiang S, Wang Q, Ma Y, Paidoula Y, et al. Sexually dimorphic tridimensionally preserved pterosaurs and their eggs. Curr Biol. 2014;24:1323–30. https://doi.org/10.1016/j.cub.2014.04.054.
2. Wang X, Kellner AWA, Jiang S, Cheng X, Wang Q, Ma Y, et al. Egg accumulation with 3D embryos provides insight into the life history of a pterosaur. Science. 2017;358:1197–201. https://doi.org/10.1126/science.aan2329.
3. Unwin DM, Deeming DC. Pterosaur eggshell structure and its implications for pterosaur reproductive biology. Zitteliana: An International Journal of Palaeontology and Geobiology. 2008;B28:199–207.
4. Lü J, Unwin DM, Deeming DC, Jin X, Liu Y, Ji Q. An egg-adult association, gender, and reproduction in pterosaurs. Science. 2011;331:321–4. https://doi.org/10.1126/science.1197323.
5. Li Y, Zhu X, Wang Q, Jiang S, Yang Y, Luo W, Wang X. Apatite in *Hamipterus tianshanensis* eggshell: advances in understanding the structure of pterosaur eggs by Raman spectroscopy. Herit Sci. 2022;10:84. https://doi.org/10.1186/s40494-022-00720-7.
6. Li Y, Luo W, Yang Y, Jiang S, Wang X. A preliminary study of the weathering mechanism of fossilized cretaceous *Hamipterus* bones. Sci China Earth Sci. 2021. https://doi.org/10.1007/s11430-020-9702-8.
7. Li Y, Luo W, Yang Y, Wang X. The weathering mechanism of surrounding rocks in *Hamipterus* fossil. Acta Palaeontol Sinica. 2019;58:515–25. https://doi.org/10.19800/j.cnki.aps.2019.04.007.
8. Han X, Zhao W, Chen C, Jiang S, Wang X. Study on the unusual weathering of the bones and eggs accumulation with embryos fossils of *Hamipterus tianshanensis*. Geol Rev. 2022;68:81–92.
9. Charola AE. Salts in the deterioration of porous materials: an overview. J Am Inst Conserv. 2000;39:327–43. https://doi.org/10.1179/019713600806113176.
10. Doehne E. Salt weathering: a selective review. Geological Society, London, Special Publications. 2002;205:51–64. https://doi.org/10.1144/gsl.Sp.2002.205.01.05.
11. Peng X, Wang Y, Ma X-F, Bao H, Huang X, Zhou H, Luo H, Wang X. Sol-Gel derived hybrid materials for conservation of fossils. J Solgel Sci Technol. 2020;94:347–55. https://doi.org/10.1007/s10971-020-05242-x.
12. Ruffolo SA, La Russa MF, Ricca M, Belfiore CM, Macchia A, Comite V, Pezzino A, Crisci GM. New insights on the consolidation of salt weathered limestone: the case study of Modica stone. Bull Eng Geol Environ. 2017;76:11–20. https://doi.org/10.1007/s10064-015-0782-1.
13. Vasanelli E, Calia A, Masieri M, Baldi G. Stone consolidation with SiO_2 nanoparticles: Effects on a high porosity limestone. Constr Build Mater. 2019;219:154–63. https://doi.org/10.1016/j.conbuildmat.2019.05.169.
14. Bracciale MP, Sammut S, Cassar J, Santarelli ML, Marrocchi A. Molecular crystallization inhibitors for salt damage control in porous materials: an overview. Molecules. 2020;25: 1873.
15. Rivas T, Feijoo J, De Rosario I, Taboada J. Use of ferrocyanides on Granite desalination by immersion and poultice-based methods. Int J Architectural Herit. 2017;11:588–606. https://doi.org/10.1080/15583058.2016.1277282.
16. Rivas T, Alvarez E, Mosquera MJ, Alejano L, Taboada J. Crystallization modifiers applied in granite desalination: the role of the stone pore structure.

Constr Build Mater. 2010;24:766–76. https://doi.org/10.1016/j.conbuildmat.2009.10.031.
17. Kjeldsen P. Behaviour of cyanides in soil and groundwater: a review. Water Air Soil Pollut. 1999;115:279–308. https://doi.org/10.1023/A:1005145324157.
18. Granneman SJC, Lubelli B, Van Hees RPJ. Mitigating salt damage in building materials by the use of crystallization modifiers: a review and outlook. J Cult Herit. 2019;40:183–94. https://doi.org/10.1016/j.culher.2019.05.004.
19. Verges-Belmin V, Siedel H. Desalination of masonries and monumental sculptures by poulticing: a review. Restor Build Monuments. 2005;11:391–408. https://doi.org/10.1515/rbm-2005-6000.
20. Rörig-Dalgaard I. Further developments of a poultice for electrochemical desalination of porous building materials: minimization of side effects. Mater Struct. 2015;48:1901–17. https://doi.org/10.1617/s11527-014-0282-y.
21. Kröner S, Alcaide BM, Mas-Barberà X. Influence of substrate pore size distribution, poultice type, and application technique on the desalination of medium-porous stones. Stud Conserv. 2016;61:286–96. https://doi.org/10.1080/00393630.2015.1131942.
22. Sawdy A, Lubelli B, Voronina V, Pel L. Optimizing the extraction of soluble salts from porous materials by poultices. Stud Conserv. 2010;55:26–40.
23. Pel L, Sawdy A, Voronina V. Physical principles and efficiency of salt extraction by poulticing. J Cult Herit. 2010;11:59–67. https://doi.org/10.1016/j.culher.2009.03.007.
24. Lubelli B, Van Hees RPJ. Desalination of masonry structures: fine tuning of pore size distribution of poultices to substrate properties. J Cult Herit. 2010;11:10–8. https://doi.org/10.1016/j.culher.2009.03.005.
25. Feijoo J, De Buergo MA, Fort R, Aly N. Experimental study of different electrokinetic configurations for desalination of a Brick Wall. In: El-Qady GM, Margottini C, editors. Sustainable conservation of UNESCO and other heritage sites through proactive geosciences. Cham, Switzerland: Springer; 2023. p. 89–104.
26. Rörig-Dalgaard I, Ottosen LM. Method and device for removing an ionic impurity from building structures. Geneva: World Intellectual Property Organization; 2009.
27. Feijoo J, Matyščák O, Ottosen LM, Rivas T, Nóvoa XR. Electrokinetic desalination of protruded areas of stone avoiding the direct contact with electrodes. Mater Struct. 2016;50:82. https://doi.org/10.1617/s11527-016-0946-x.
28. Feijoo J, Rivas T, Nóvoa XR, De Rosario I, Otero J. In situ desalination of a granitic column by the electrokinetic method. Int J Architectural Herit. 2018;12:63–74. https://doi.org/10.1080/15583058.2017.1370509.
29. Feijoo J, Nóvoa XR, Rivas T, Mosquera MJ, Taboada J, Montojo C, Carrera F. Granite desalination using electromigration. Influence of type of granite and saline contaminant. J Cult Herit. 2013;14:365–76. https://doi.org/10.1016/j.culher.2012.09.004.
30. Ottosen L, V Christensen I, Rörig-Dalgaard I. Electrochemical desalination of salt infected limestone masonry of a historic warehouse. In: Proceedings of structural faults and repair; Edinburgh. 2012.
31. Ottosen L, Rörig-Dalgaard I, Villumsen A. Electrochemical removal of salts from masonry – Experiences from pilot scale. In: Proceedings of the Proceedings of the international conference salt weathering on buildings and stone sculptures. Copenhagen; 2008. p. 341–350.
32. Ishaq M, Kamran K, Jamil Y, Sarfraz RA. Electric potential and current distribution in contaminated porous building materials under electrokinetic desalination. Mater Struct. 2021;54:175. https://doi.org/10.1617/s11527-021-01770-2.
33. Awan FUR, Al-Yaseri A, Akhondzadeh H, Iglauer S, Keshavarz A. Influence of mineralogy and surfactant concentration on zeta potential in intact sandstone at high pressure. J Colloid Interface Sci. 2022;607:401–11. https://doi.org/10.1016/j.jcis.2021.08.015.
34. Maitschke J, Siedel H. Desalination of Cotta type Elbe sandstone with adapted poultices: Optimization of poultice mixtures. In: Proceedings of the Proceedings of SWBSS 2017. Fourth International Conference on Salt Weathering of Buildings and Stone Sculptures, Potsdam, Germany; 2017. p. 208–218.
35. Baker JC, Uwins PJR, Mackinnon IDR. ESEM study of illite/smectite freshwater sensitivity in sandstone reservoirs. J Petrol Sci Eng. 1993;9:83–94. https://doi.org/10.1016/0920-4105(93)90069-Q.
36. 3355-1. ÖNORM B. Trockenlegung von feuchtem Mauerwerk – Teil 1:bauwerksdiagnose und Planungsgrundlagen Berlin. ASI Austrian Standards Institute Österreichisches Normungsinstitut, Herausgeber Deutschland; 2006.
37. Randazzo L, Montana G, Castiglia A, La Russa MF. Salt extraction from lime-based mortars: an experimental study using different poultice formulations. Constr Build Mater. 2020;255: 119391. https://doi.org/10.1016/j.conbuildmat.2020.119391.
38. Vučetic S, Ranogajec J, Hirschenberger H, Van Der Bergh JM, Vidaković A, Markov S. Cleaning and protection of historic objects – biotechnology and nanotechnology approach. IOP Conference Series: Materials Science and Engineering. 2018;364: 012071. https://doi.org/10.1088/1757-899X/364/1/012071.
39. Sētiņa J, Kirilova S. Clay based poultices for desalination of building materials. J Sustainable Archit Civil Eng. 2012;1:52–7.
40. Matyščák O. Desalination of salt damaged Obernkirchen sandstone by an applied DC field. Constr Building Mater. 2014;71:561–9.
41. Ottosen LM, Dias-Ferreira C, Ribeiro AB. Electrochemical desalination of historic portuguese tiles – removal of chlorides, nitrates and sulfates. J Cult Herit. 2015;16:712–8. https://doi.org/10.1016/j.culher.2014.11.003.
42. Ottosen LM, Ferreira CMD, Christensen IV. Electrokinetic desalination of glazed ceramic tiles. J Appl Electrochem. 2010;40:1161–71. https://doi.org/10.1007/s10800-010-0086-x.
43. Ottosen LM, Hansen HK. Electro-desalination of buildings suffering from salt weathering. In: Ribeiro AB, Mateus EP, Couto N, editors. Electrokinetics across disciplines and continents: new strategies for sustainable development. Cham: Springer International Publishing; 2016. p. 205–24.
44. Zhang Y, Xu J, Yang G. Multi-ion migration of Ca^{2+}, Mg^{2+}, Na^{+} and K^{+} in the CREDI process. Sep Sci Technol. 2016;51:1210–9. https://doi.org/10.1080/01496395.2016.1147466.
45. Pazgarcia JM, Johannesson B, Ottosen LM, Ribeiro AB, Rodriguezmaroto JM. Simulation-based analysis of the differences in the removal rate of chlorides, nitrates and sulfates by electrokinetic desalination treatments. Electrochim Acta. 2013;89:436–44.
46. Bhattacharyya KG, Gupta SS. Adsorption of a few heavy metals on natural and modified kaolinite and montmorillonite: a review. Adv Colloid Interface Sci. 2008;140:114–31. https://doi.org/10.1016/j.cis.2007.12.008.
47. Delgado JR, Grossi A. Indicators and ratings for the compatibility assessment of conservation actions. J Cult Herit 2007;8(1):32–43. https://doi.org/10.1016/j.culher.2006.04.007.
48. Tripathy S, Rao KSS. Cyclic swell–shrink Behaviour of a compacted expansive soil. Geotech Geol Eng. 2009;27:89–103.
49. Feijoo J, De Rosario I, Rivas T, Mosquera MJ, Benavides R. Influence of a pre-consolidation treatment on the desalination effectiveness of a highly deteriorated Granite Façade of medieval age. Int J Architectural Herit. 2022. https://doi.org/10.1080/15583058.2022.2086506.
50. Correia J, Matero F. Calcium tartrate tetrahydrate preconsolidation of salt-contaminated limestone at mission San José Y San Miguel De Aguayo. J Am Inst Conserv. 2008;47:81–95. https://doi.org/10.1179/019713608806112160.
51. Feijoo J, Fort R, Gomez-Villalba LS, Rabanal ME, Ottosen LM. Electroprecipitation of magnesium and calcium compounds for weathering protection of ornamental rocks. Cryst Growth Des. 2020;20:2337–55. https://doi.org/10.1021/acs.cgd.9b01497.
52. Gomez-Villalba LS, Feijoo J, Rabanal ME, Fort R. In-situ electrochemical synthesis of inorganic compounds for materials conservation: assessment of their effects on the porous structure. Ceram Int. 2021;47:30406–24. https://doi.org/10.1016/j.ceramint.2021.07.221.
53. Feijoo J, Nóvoa XR, Rivas T. Electrokinetic treatment to increase bearing capacity and durability of a granite. Mater Struct. 2017;50:251. https://doi.org/10.1617/s11527-017-1123-6.

Publisher's Note